DISCRETE STATE FEEDBACK CONTROL OF A FURUTA PENDULUM USING STATE ESTIMATOR

Luiz Eduardo Pivovar[1], Uiliam Nelson Lendzion Tomaz Alves[1], Ricardo Breganon[1], Rodrigo Henrique Cunha Palácios[2] and Márcio Mendonça[2]
[1]Instituto Federal do Paraná (IFPR), Av. Dr. Tito, Jacarezinho, Paraná, Brazil.
luiz.pivovar@ifpr.edu.br; uiliam.alves@ifpr.edu.br;
ricardo.breganon@ifpr.edu.br
[2]Universidade Tecnológica Federal do Paraná (UTFPR), Av. Alberto Carazzai, Cornélio Procópio, Paraná, Brazil.
rodrigopalacios@utfpr.edu.br; mendonca@utfpr.edu.br

ABSTRACT

The Furuta Pendulum is a mechanical system designed to simulate the problem of self-balancing. It consists of a motor, an arm, and a rod connected by rotational joints. Its control challenge involves stabilizing the rod above its rotational axis in an equilibrium position. The Furuta Pendulum's multivariable and highly nonlinear dynamics make it suitable for comparison to problems with significant connections to industry and society, such as stabilizing bipedal robots, individual transport vehicles, and modelling buildings to study the impact of earthquakes on their structures. This paper presents the construction of a Furuta Pendulum prototype and its mathematical modeling using the Lagrangian formulation. State feedback control designs were developed to stabilize the pendulum using Pole Placement and Linear Quadratic Regulator (LQR) techniques. Since the controllers are implemented via a digital computer, the Analog/Digital and Digital/Analog converters in the control loop were considered in the controller's design by describing the system's dynamics in discrete time and using discrete-time control techniques. State estimators were also implemented to estimate the state variables needed for feedback that are not physically measured in the prototype. The performances of the controllers were compared through graphical analysis and the ITAE (Integral of Time Multiplied by Absolute Error) index. The results indicated that both controllers were able to stabilize the pendulum's rod in a vertical position and make the system arm follow a specific reference. The LQR controller showed a slightly more satisfactory performance than the Pole Placement controller, with smaller amplitudes of oscillation around the reference in the practical experiments and a shorter time to reach equilibrium in the simulations.

KEYWORDS: *Furuta Pendulum, Lagrangian Modeling, Pole Placement, Linear Quadratic Regulator (LQR), Discrete-time control.*

I. INTRODUCTION

The Rotational Pendulum, also known as a Furuta Pendulum, is a type of inverted pendulum developed by Katsuhisa Furuta and his team in 1992 as a didactic tool for the study of control techniques [1]. This system consists of a motor, an arm, and a rod. The motor is coupled to one end of the arm. The arm stands in a horizontal position, and the motor generates the rotation movement of the set. At the other end of the arm, an articulated rod is positioned, performing the function of a pendulum. Therefore, this device has two rotational joints that define the number of degrees of freedom of the system and contains only one control input [2].

The main challenge inherent to this mechanical system is to stabilize the rod above its rotational axis in a vertical position. In this way, the pendulum should stay balanced around the point of operation. The Furuta Pendulum also stands out for being a multivariable underactuated system and for presenting nonlinear dynamic characteristics [3].

Due to these characteristics, stabilizing the Furuta Pendulum in the vertical position has become a classic problem in the control field, and it has motivated the development of several studies. Different control techniques can be used to solve this problem. For example, [4] simulated a Pole Placement via state feedback control of a Furuta Pendulum. The Linear Quadratic Regulator (LQR) technique was used to control this system in [5], and a predictive controller was considered in [6, 7]. The authors in [8, 9] explored the use of an adaptive neural network to control a Furuta Pendulum, and [10] applied an integral plus proportional controller (PIP). Sliding mode control was employed in [11, 12]. An adaptive frame of reference model combined with a PID controller was considered in [2]. The papers [13, 14] applied H∞ control to Furuta Pendulums. Finally, a Fuzzy-PID method was employed in [15, 16].

Despite its simple construction and didactic purpose [17], the Furuta Pendulum resembles mechanical systems relevant to society and industry. For instance, modeling bipedal robots [18] and controlling rocket's launch [19] is worth mentioning. Additionally, the control of individual vehicles using the Furuta Pendulum has been explored in [20], and NASA has also conducted studies on autonomous robots based on this system [21]. Finally, the control of vibrations in structures can be analyzed by modeling an inverted pendulum [22]. From this perspective, the results obtained at the prototype level can serve as a reference for real systems.

The object of study of this work consists of a Furuta Pendulum prototype installed in the Industrial Automation and Control laboratory of the Federal Institute of Paraná, Jacarezinho, Paraná, Brazil, which was designed together with the Federal Technological University of Paraná, Cornélio Procópio, Paraná, Brazil. The relevant parameters of the motor used in the prototype, such as the armature inductance, armature resistance, motor shaft, and damping constants were obtained through experiments [23].

This paper presents the mathematical modeling of the Furuta Pendulum, which was analytically carried out using the Lagrangian formulation. Furthermore, two discrete-time state feedback controllers were designed to stabilize the system's pendulum in the vertical position using Pole Placement and LQR techniques, respectively. The mathematical modeling, as well as the controller designs, were validated through simulations and experiments. Finally, graphical analysis and ITAE index compared the controllers' performance.

Although the Furuta Pendulum presents nonlinear dynamics, as previously mentioned, many works employ a linear approximation of its model in the controller design. In this sense, some relevant results are found in [13, 15, 24–26]. It is important to point out that this work also considers a linear model to design the controllers so that the system's operation is restricted to the vicinity of its operating point. The prototype measures only the rod's and arm's angles. Due to this, to implement the state feedback strategies, state estimators were designed based on the linear model of the system [27] and used with the controllers.

The rest of the paper is divided as follows. Section 2 presents the prototype's structural aspects and indicates the system's parameters and variables. Section 3 describes the mathematical model of the Furuta Pendulum. The design of the controllers is presented in Section 4. Section 5 presents the results. Finally, Section 6 concludes and suggests possible future work.

II. FURUTA PENDULUM PROTOTYPE

Figure 1 shows a diagram of the Furuta Pendulum prototype used in this work. In this figure, $\theta_1(t)$ represents the angle of the Pendulum's arm measured in a horizontal plane, whose direction is determined by the axis $\hat{X}_0$ of the inertial coordinate system $\{0\}$. The angle $\theta_2(t)$ represents the angle of the Pendulum's rod, and it is measured in a vertical plane between the pendulum rod and the axis $\hat{X}_2$ of the coordinate system $\{2\}$. $v(t)$ represents the voltage applied to the motor. In this prototype, both angles $\theta_1(t)$ and $\theta_2(t)$ are measured by sensors and are available for feedback, while the voltage $v(t)$ is the control signal.

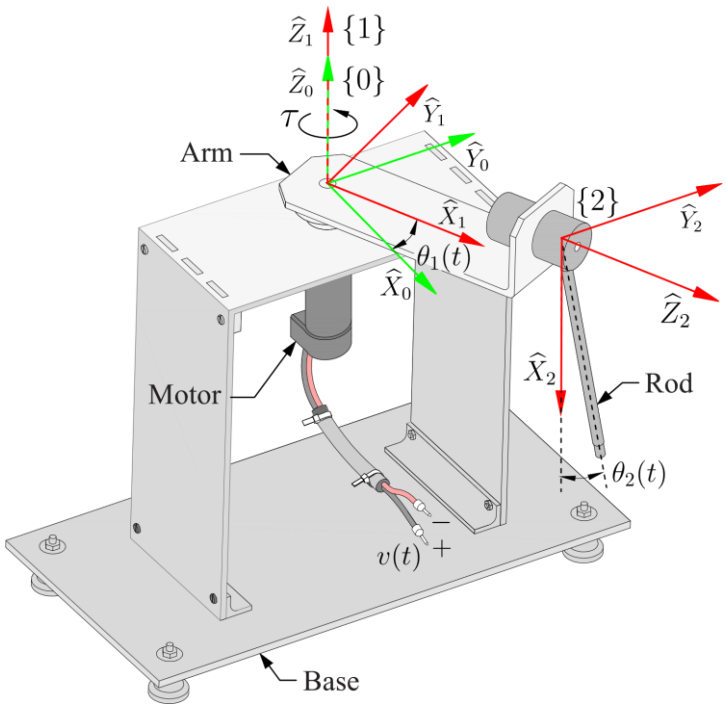

Figure 1. Diagram of the Furuta Pendulum prototype.

The motor supplies the torque to the arm and generates a combined movement between the arm and the rod, allowing the rod to oscillate freely around its axis of rotation, $\hat{Z}_2$. The main objective of the controller of this system is to apply an adequate voltage to the motor so that the rod remains around the vertical position, defined by $\theta_2(t) = \pi\, rad$.

Figure 2 shows the bench setup used in the experiments, where numbers are used to identify the main components. The prototype of the Furuta Pendulum is labeled as ⑤. The system's rotation is generated by a brushless $12\ V\ DC$ motor manufactured by Maxon®. An incremental encoder of $500\ PPR$ (Pulses per Revolution) is installed on the motor shaft, whose function is to measure the arm's angular position, $\theta_1(t)$. The prototype's arm is made of aluminum and is attached to the motor shaft at one end. At the other end of the arm, there is a $600\ PPR$ incremental encoder, which aims to measure the angle of the rod position, $\theta_2(t)$. The rod is a cylindrical and thin component made of aluminum, which performs the pendulum function in the system. This component is coupled to the motor's arm by a nylon cylinder.

The voltages supplied to the motor and encoders are provided by a $12\ V$ and a $5\ V\ DC$ power supplies, ① and ⑥, respectively.

The data acquisition system, which is responsible for providing signals from the sensors to the computer and sending control actions to the actuators, consists of a National Instruments® NI-PCI 6602 board (located inside the computer) and a connector block labeled as ④. The controller is implemented using MatLab/Simulink® software and runs on an Intel(R) Core (TM) Duo $E8600$ processor clocked at $3.33\ GHz$ with $2\ GB$ installed memory ②.

The control signal is sent to the H-bridge ③, which converts it into an equivalent voltage that powers the motor. In consequence, it controls the direction and speed of movement. The controller aims to stabilize the rod in the inverted position ($\theta_2(t) = \pi\, rad$), even when the system is subject to disturbances or changes in the arm angle. Controllers based on Pole Placement and LQR techniques were designed, simulated, and applied to the prototype shown in Figure 2. These controllers' design and implementation details are presented after the mathematical model of this system in the next section.

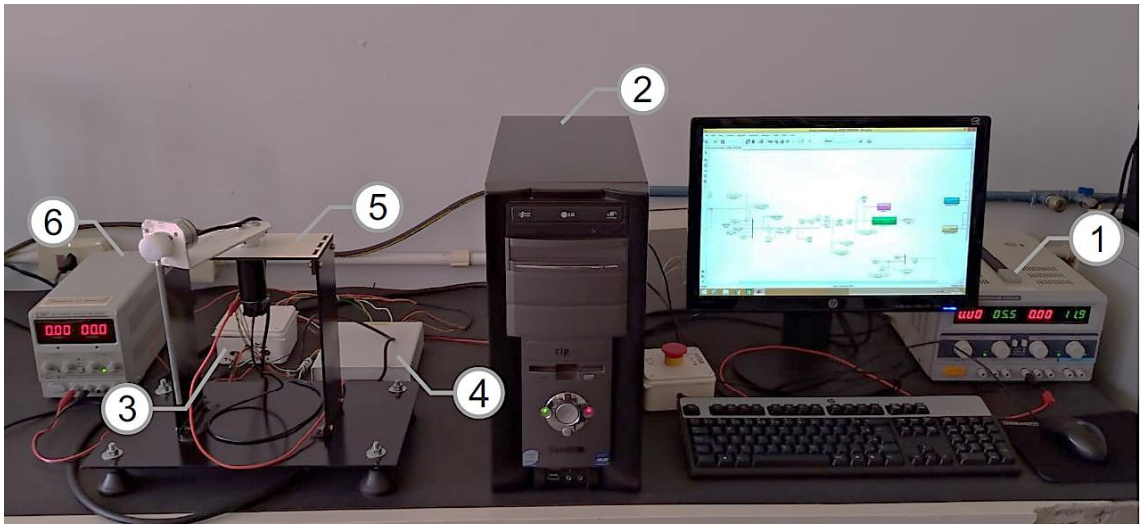

Figure 2. Furuta Pendulum prototype available at the Industrial Automation and Control Laboratory of the Federal Institute of Paraná, Jacarezinho, Paraná, Brazil.

III. MATHEMATICAL MODEL

Figure 3 presents the coordinate systems and defines the main variables, parameters, and states of the Furuta pendulum. As can be seen, the reference system is composed of the inertial (static) coordinate system {0}. The origin is located on the motor's axis, constituted by the vectors $\hat{X}_0$, $\hat{Y}_0$, and $\hat{Z}_0$.

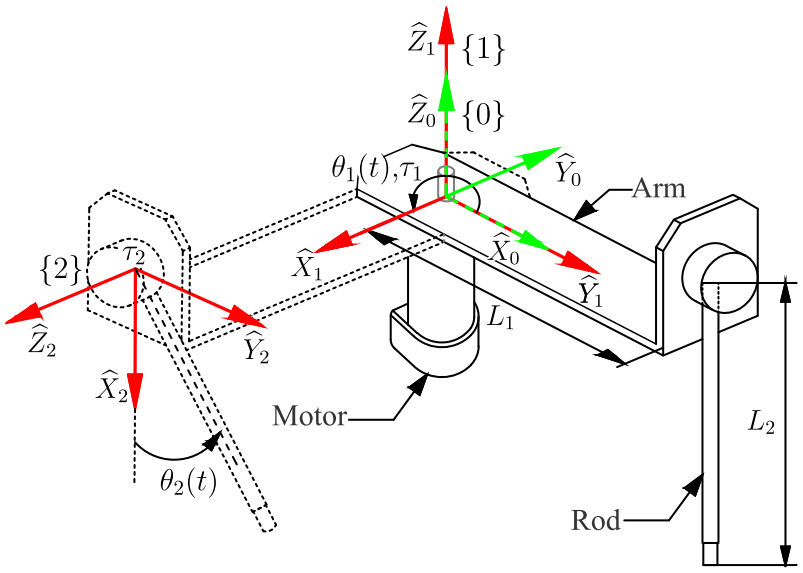

Figure 3. Furuta Pendulum reference system.

The coordinate system {1} can also be observed in Figure 3. It consists of the unit vectors $\hat{X}_1$, $\hat{Y}_1$ and $\hat{Z}_1$, with the same origin as the system {0}. However, the coordinate system {1} is rotated by the angle θ_1 around the axis $\hat{Z}_0$ regarding to the system {0}. Thus, the location of the system {1} in relation to {0} is determined by the rotation matrix [28]

$$ {}^{0}_{1}R = \begin{bmatrix} \cos(\theta_1) & \sin(\theta_1) & 0 \\ -\sin(\theta_1) & \cos(\theta_1) & 0 \\ 0 & 0 & 1 \end{bmatrix}. $$

Finally, the coordinate system {2} is made up of the unit vectors $\hat{X}_2$, $\hat{Y}_2$, and $\hat{Z}_2$, originating from the rod's rotational axis (see Figure 3). This system has a rotation of $\pi/2$ rad around the axis $\hat{Y}_1$ and a magnitude shift of L_1 with respect to the origin of the system {0}. The coordinate system transformation matrix from {2} to {0} is determined by the product of a rotation matrix of angle θ_2 and a matrix that considers the translation between these two systems [28], which gives

$$ {}^0_2R = \begin{bmatrix} \cos(\theta_2) & \sin(\theta_2) & 0 \\ -\sin(\theta_2) & \cos(\theta_2) & 0 \\ 0 & 0 & 1 \end{bmatrix} \begin{bmatrix} 0 & 0 & -1 \\ 0 & 1 & 0 \\ L_1 & 0 & 0 \end{bmatrix} = \begin{bmatrix} 0 & \sin(\theta_2) & -\cos(\theta_2) \\ 0 & \cos(\theta_2) & \sin(\theta_2) \\ L_1 & 0 & 0 \end{bmatrix}. \quad (1) $$

The Furuta Pendulum shown in Figure 2 has one main axis along the arm $\hat{X}_1$, and the other two principal axes located in a plane perpendicular to the arm ($\hat{Y}_1$ and $\hat{Z}_1$). These three axes are mutually orthogonal. Thus, the inertia tensor of the pendulum arm is [29]

$$ J_1 = \begin{bmatrix} J_{1xx} & 0 & 0 \\ 0 & J_{1yy} & 0 \\ 0 & 0 & J_{1zz} \end{bmatrix}, \quad (2) $$

where J_{1xx}, J_{1yy}, and J_{1zz} are the moments of inertia about the principal axes $\hat{X}_1$, $\hat{Y}_1$ and $\hat{Z}_1$, respectively. The pendulum's rod, in turn, is defined in the main axes of the system {2} ($\hat{X}_2$, $\hat{Y}_2$, $\hat{Z}_2$), so the inertia tensor is defined as [29]

$$ J_2 = \begin{bmatrix} J_{2xx} & 0 & 0 \\ 0 & J_{2yy} & 0 \\ 0 & 0 & J_{2zz} \end{bmatrix}, \quad (3) $$

where J_{2xx}, J_{2yy}, and J_{2zz} are the moments of inertia about the principal axes $\hat{X}_2$, $\hat{Y}_2$, and $\hat{Z}_2$, respectively.

The kinetic and potential energies are used in the Lagrangian formulation. Therefore, these energies need to be calculated. The angular velocity is incorporated in the kinetic energy of the system, which, for the arm, is given by

$$ \omega_1 = [0 \quad 0 \quad \dot{\theta}_1]^T \quad (4) $$

Considering that the system starts from the rest, the initial velocity of the arm is $\mathrm{v}_1 = [0 \quad 0 \quad 0]^T$. The total linear velocity of the center of mass of the arm is given by the sum of the initial velocity of the arm and the vector product of the angular velocity and the position vector, i. e.,

$$ \mathrm{v}_{1c} = \mathrm{v}_1 + \omega_1 \times [l_1 \quad 0 \quad 0]^T = [0 \quad \dot{\theta}_1 l_1 \quad 0]^T, \quad (5) $$

where l_1 represents the distance between the center of mass of the arm and the motor shaft. For the prototype, this distance corresponds to half the length of the arm, that is, $l_1 = L_1/2$.

The angular velocity of the rod with reference to coordinate system {0}, using (1), is given by

$$ \omega_2 = {}^0_2R \times \omega_1 + [0 \quad 0 \quad \dot{\theta}_2]^T = [-\cos(\theta_2)\dot{\theta}_1 \quad \sin(\theta_2)\dot{\theta}_1 \quad \dot{\theta}_2]^T. \quad (6) $$

The velocity of the joint between the arm and the rod in the initial position is $\omega_1 \times [L_1 \quad 0 \quad 0]^T$. So, the speed of the rod in the final position can be calculated with reference to the system {0} employing (1):

$$ \mathrm{v}_2 = {}^0_2R \times \omega_1 \times [L_1 \quad 0 \quad 0]^T = \begin{bmatrix} \dot{\theta}_1 L_1 \sin(\theta_2) \\ \dot{\theta}_1 L_1 \cos(\theta_2) \\ 0 \end{bmatrix}. \quad (7) $$

The total linear velocity of the center of mass of the rod, using (6) and (7), is given by

$$\mathrm{v}_{2c} = \mathrm{v}_2 + \omega_2 \times [l_2 \quad 0 \quad 0]^T = \begin{bmatrix} \dot{\theta}_1 L_1 \sin(\theta_2) \\ \dot{\theta}_1 L_1 \cos(\theta_2) + \dot{\theta}_2 l_2 \\ -\dot{\theta}_1 l_2 \sin(\theta_2) \end{bmatrix}. \tag{8}$$

During the movement, the height of the arm does not change, since it has no vertical movement. As a result, the potential energy of the arm is [30]

$$E_{p1} = 0. \tag{9}$$

To define the kinetic energy of the arm, the rotation and translation movements of this component are considered [30], then, by using (6), (2) and (4),

$$E_{k1} = \frac{1}{2}(\mathrm{v}_{1c}^T m_1 \mathrm{v}_{1c} + \omega_1^T J_1 \omega_1) = \frac{1}{2}\dot{\theta}_1^2(m_1 l_1^2 + J_{1zz}), \tag{10}$$

where m_1 corresponds to the mass of the arm.

For the rod, there is variation in height due to its rotation movement in a vertical plane. The height of the rod's center of mass depends on the angle θ_2 and it is given by $l_2(1 - \cos(\theta_2))$, where l_2 is the distance from the origin of the coordinate system $\{2\}$ to the rod's center of mass. Therefore, the potential energy of this component is [30]

$$E_{p2} = g m_2 l_2 \big(1 - \cos(\theta_2)\big), \tag{11}$$

where m_2 corresponds to the mass of the rod.

The kinetic energy of the rod is also defined from the rotation and translation movements [30], so

$$E_{k2} = \frac{1}{2}(\mathrm{v}_{2c}^T m_2 \mathrm{v}_{2c} + \omega_2^T J_2 \omega_2). \tag{12}$$

Then, by using (3), (7) and (8), (12) can be written as

$$E_{k2} = \frac{1}{2}\dot{\theta}_1^2 \left[m_2 L_2^2 + \left(m_2 l_2^2 + J_{2yy} \right) \sin^2(\theta_2) + J_{2xx} \cos^2(\theta_2) + \frac{1}{2}\dot{\theta}_2^2 J_{2zz} + m_2 l_2^2 \right] + m_2 L_1 l_2 \cos(\theta_1)\, \dot{\theta}_1 \dot{\theta}_2. \tag{13}$$

The potential energy and total kinetic energy of the system are

$$E_p = E_{p1} + E_{p2}, \tag{14}$$

$$E_k = E_{k1} + E_{k2}. \tag{15}$$

The Lagrangian function is defined as the difference between the kinetic energy and the potential energy of the system [31]:

$$L = E_k - E_p. \tag{16}$$

The Euler Lagrange equation, considering the viscosity of the system, is given by [31]

$$\frac{d}{dt}\left(\frac{\partial L}{\partial \dot{q}_i}\right) + b_i \dot{q}_i - \frac{\partial L}{\partial q_i} = Q_i, \tag{17}$$

where $q_i = [\theta_1, \quad \theta_2]^T$ is the generalized coordinate vector, $b_i = [b_1, \quad b_2]^T$ represents the vector of the generalized viscous damping coefficients and $Q_i = [\tau_1, \quad \tau_2]^T$ is the vector of generalized forces (torques).

In order to solve (17), first consider the terms $\frac{d}{dt}\left(\frac{\partial L}{\partial \dot{q}_i}\right)$ and $-\frac{\partial L}{\partial q_i}$ for each variable $q_1 = \theta_1$ and $q_2 = \theta_2$. Based on (11)-(17), these terms are calculated as

$$\frac{d}{dt}\left(\frac{\partial L}{\partial \dot{\theta}_1}\right) = \ddot{\theta}_1[J_{1zz} + m_1 l_1^2 + m_2 L_1^2 + (m_2 l_2^2 + J_{2yy})\sin^2(\theta_2) + J_{2xx}\cos^2(\theta_2)] + m_2 L_1 l_2 \cos(\theta_2)\,\ddot{\theta}_2 - m_2 L_1 l_2 \sin(\theta_2)\,\dot{\theta}_2^2 + \dot{\theta}_1\dot{\theta}_2 \sin(2\theta_2)(m_2 l_2^2 + J_{2yy} - J_{2xx}). \quad (18)$$

$$\frac{d}{dt}\left(\frac{\partial L}{\partial \dot{\theta}_2}\right) = \ddot{\theta}_1 m_2 L_1 l_2 \cos(\theta_2) + \ddot{\theta}_2(J_{2zz} + m_2 l_2^2) - \dot{\theta}_1\dot{\theta}_2 m_2 L_1 l_2 \sin(\theta_2). \quad (19)$$

$$-\frac{\partial L}{\partial \theta_1} = 0. \quad (20)$$

$$-\frac{\partial L}{\partial \theta_2} = -\frac{1}{2}\dot{\theta}_1^2 \sin(2\theta_2)(m_2 l_2^2 + J_{2yy} - J_{2xx}) + \dot{\theta}_1\dot{\theta}_2 m_2 L_1 l_2 \sin(\theta_2) + g m_2 l_2 \sin(\theta_2). \quad (21)$$

The pendulum used in this work has long and thin arm and rod, which enable the moment of inertia along the axis of these components to be neglected. Additionally, the pendulum has rotational symmetry, so the moments of inertia about two of its main axes are almost equal. As a result, it is possible to obtain an approximation of the inertia tensors (2) and (3), as described in [32], as

$$J_1 = \begin{bmatrix} J_{1xx} & 0 & 0 \\ 0 & J_{1yy} & 0 \\ 0 & 0 & J_{1zz} \end{bmatrix} \approx \begin{bmatrix} 0 & 0 & 0 \\ 0 & J_1 & 0 \\ 0 & 0 & J_1 \end{bmatrix},$$
$$J_2 = \begin{bmatrix} J_{2xx} & 0 & 0 \\ 0 & J_{2yy} & 0 \\ 0 & 0 & J_{2zz} \end{bmatrix} \approx \begin{bmatrix} 0 & 0 & 0 \\ 0 & J_2 & 0 \\ 0 & 0 & J_2 \end{bmatrix}. \quad (22)$$

According to the parallel axis theorem, the moment of inertia of the arm about its axis of rotation is

$$\hat{J}_1 = J_1 + m_1 l_1^2. \quad (23)$$

For the rod, the moment of inertia is defined as

$$\hat{J}_2 = J_2 + m_2 l_2. \quad (24)$$

Finally, the total moment of inertia that the motor experiences when the rod is in its equilibrium position ($\theta_2(t) = 0$ in Figure 3) is

$$\hat{J}_0 = \hat{J}_1 + m_2 L_1^2 = J_1 + m_1 l_1^2 + m_2 L_1^2\,. \quad (25)$$

Applying (18)-(25) in the Euler Lagrange equation (17) results in [32]:

$$\begin{bmatrix} \ddot{\theta}_1[\hat{J}_0 + \hat{J}_2 \sin^2(\theta_2)] + \ddot{\theta}_2 m_2 L_1 l_2 \cos(\theta_2) \\ -m_2 L_1 l_2 \sin(\theta_2)\dot{\theta}_2^2 + \dot{\theta}_1\dot{\theta}_2 \hat{J}_2 \sin(2\theta_2) + b_1\dot{\theta}_1 \\ \ddot{\theta}_1 m_2 L_1 l_2 \cos(\theta_2) + \ddot{\theta}_2 \hat{J}_2 + \frac{1}{2}\dot{\theta}_2^2 \hat{J}_2 \sin(2\theta_2) \\ +b_2\dot{\theta}_2 + g m_2 l_2 \sin(\theta_2) \end{bmatrix} = \begin{bmatrix} \tau_1 \\ \tau_2 \end{bmatrix}. \quad (26)$$

The Pendulum is driven by a DC motor attached to one end of the arm. The torque provided by this motor is $\tau(t) = K_m.i(t)$, where $i(t)$ the electric current in the motor armature and K_m the motor constant. Besides, consider that there are external torques $\bar{\tau}_1(t)$ and $\bar{\tau}_2(t)$ acting on the arm and rod axes, respectively. So, it follows that

$$\tau_1 = K_m i(t) + \bar{\tau}_1(t), \quad (27)$$

$$\tau_2 = \bar{\tau}_2(t). \quad (28)$$

Using (27) and (28), (26) can be written as

$$\begin{bmatrix} M_{11} & M_{12} \\ M_{12} & \hat{J}_2 \end{bmatrix}\begin{bmatrix} \ddot{\theta}_1 \\ \ddot{\theta}_2 \end{bmatrix} = -\begin{bmatrix} C_{11} & C_{12} \\ C_{21} & b_2 \end{bmatrix}\begin{bmatrix} \dot{\theta}_1 \\ \dot{\theta}_2 \end{bmatrix} + \begin{bmatrix} K_m i(t) + \bar{\tau}_1(t) \\ \bar{\tau}_2(t) \end{bmatrix} - \begin{bmatrix} 0 \\ \tau_0(t) \end{bmatrix}, \quad (29)$$

where

$$M_{11} = \hat{J}_0 + \hat{J}_2 \sin^2(\theta_2),$$
$$M_{12} = m_2 L_1 l_2 \cos(\theta_2),$$
$$C_{11} = b_1 + \frac{1}{2}\dot{\theta}_2 \hat{J}_2 \sin(2\theta_2),$$
$$C_{12} = \frac{1}{2}\dot{\theta}_1 \hat{J}_2 \sin(2\theta_2) - m_2 L_1 l_2 \sin(\theta_2)\dot{\theta}_2,$$
$$C_{21} = -\frac{1}{2}\dot{\theta}_1 \hat{J}_2 \sin(2\theta_2),$$
$$\tau_0(t) = g m_2 l_2 \sin(\theta_2).$$

In addition, the differential equation that describes a DC motor can be defined from Kirchhoff's law as [23]

$$L_m \frac{di}{dt}(t) = -R_m i(t) - K_m \dot{\theta}_1 + v(t), \tag{30}$$

where L_m represents the inductance in the armature of the motor, R_m is the armature resistance of the motor, and $v(t)$ the voltage that drives the motor.

Based on (30) and (29), let $x_1(t) = \theta_1(t)$, $x_2(t) = \theta_2(t)$, $x_3(t) = \dot{\theta}_1(t)$, $x_4(t) = \dot{\theta}_2(t)$ and $x_5(t) = i(t)$ be the state variables of the Furuta Pendulum dynamics, and $u(t) = v(t)$ be its control signal.

As previously mentioned, the dynamics of the system will be linearized around the operating point $x(0) = [x_1(0) \quad x_2(0) \quad x_3(0) \quad x_4(0) \quad x_5(0)]^T = [0 \quad \pi \quad 0 \quad 0 \quad 0]^T$ for the design of the controllers. Due to this, the system must remain around the operation point when functioning, that is, the pendulum must oscillate within a very small range close to the desired position. This deviation of the pendulum's position from the equilibrium point is represented by $\Delta\theta_2(t)$. As a result, one has $\cos(\theta_2) = \cos(\pi \pm \Delta\theta_2(t)) \approx 1$ and $\sin(\theta_2) = \sin(\pi \pm \Delta\theta_2(t)) \approx \Delta\theta_2(t)$.

Therefore, (29) and (30) lead to the linearized state space dynamics given by

$$\dot{x}(t) = \bar{A}x(t) + \bar{B}u(t) + \bar{D}\bar{\tau}(t), \tag{31}$$

where

$$x(t)^T = [x_1(t) \quad x_2(t) \quad x_3(t) \quad x_4(t) \quad x_5(t)],$$
$$\bar{A} = \begin{bmatrix} 0 & 0 & 1 & 0 & 0 \\ 0 & 0 & 0 & 1 & 0 \\ 0 & A_{32} & A_{33} & A_{34} & A_{35} \\ 0 & A_{42} & A_{43} & A_{44} & A_{45} \\ 0 & 0 & -\frac{K_m}{L_m} & 0 & -\frac{R_m}{L_m} \end{bmatrix}, \quad \bar{B} = \begin{bmatrix} 0 \\ 0 \\ 0 \\ 0 \\ \frac{1}{L_m} \end{bmatrix},$$
$$\bar{D} = \frac{1}{den}\begin{bmatrix} 0 & 0 & \hat{J}_2 & m_2 L_1 l_2 & 0 \\ 0 & 0 & m_2 L_1 l_2 & \hat{J}_0 & 0 \end{bmatrix}^T, \quad \bar{\tau}(t) = \begin{bmatrix} \bar{\tau}_1(t) \\ \bar{\tau}_2(t) \end{bmatrix},$$
$$A_{32} = \frac{g m_2^2 l_2^2 L_1}{den}, \quad A_{33} = -\frac{b_1 \hat{J}_2}{den}, \quad A_{34} = -\frac{b_2 m_2 l_2 L_1}{den}, \quad A_{35} = \frac{\hat{J}_2 K_m}{den},$$
$$A_{42} = \frac{g m_2 l_2 \hat{J}_0}{den}, \quad A_{43} = -\frac{b_1 m_2 l_2 L_1}{den}, \quad A_{44} = -\frac{b_2 \hat{J}_0}{den}, \quad A_{45} = -\frac{m_2 L_1 l_2 K_m}{den},$$
$$den = \hat{J}_0 \hat{J}_2 - m_2^2 L_1^2 l_2^2.$$

The acquisition board used in the prototype described in Section 2 has a sampling period of $T_s = 0.02s$. The plant dynamics were represented in discrete time using the ZOH (Zero-Order Hold) method [27] to take into account the effect of the A/D and D/A converters.

This method provides the discrete model matrices as $\Phi = e^{\bar{A}T_s}$, $\Gamma = \int_0^{T_s} e^{\bar{A}\eta}\, d\eta \bar{B}$ and $\Psi = \int_0^{T_s} e^{\bar{A}\eta}\, d\eta \bar{D}$ (considering step-like disturbances). Thus, the new matrices depend on the sampling time, T_s. The dynamics (31) are described in discrete time as

$$\begin{aligned} \xi(k+1) &= \Phi\xi(k) + \Gamma u(k) + \Psi d(k), \\ z(k) &= \Lambda\xi(k), \\ y(k) &= H\xi(k), \\ \xi(k) &= [\xi_1(k) \quad \xi_2(k) \quad \xi_3(k) \quad \xi_4(k) \quad \xi_5(k)]^T, \\ d(k) &= [d_1(k) \quad d_2(k)]^T, \quad y(k) = [y_1(k) \quad y_2(k)]^T, \end{aligned} \tag{32}$$

where $\xi_1(k)$, $\xi_2(k)$, $\xi_3(k)$, $\xi_4(k)$ and $\xi_5(k)$ are the samples of $x_1(t)$, $x_2(t)$, $x_3(t)$, $x_4(t)$ and $x_5(t)$ at each instant kT_s, respectively. $d_1(k)$ and $d_2(k)$ are the samples of $\bar{\tau}_1(t)$ and $\bar{\tau}_2(t)$; $y_1(t)$ and $y_2(t)$ are the measured outputs, and $z(k)$ is the controlled output.

The matrices presented in the model of the discrete time system (32) depend on the system parameters, which values and units are indicated in Table 1. Using the values in Table 1, the matrices in (32) are calculated as follows

$$\begin{aligned} \Phi &= \begin{bmatrix} 1 & 0.0010 & 0.0199 & -0.0000 & 0.0001 \\ 0 & 1.0157 & -0.0001 & 0.0198 & 0.0001 \\ 0 & 0.0959 & 0.9937 & -0.0008 & 0.0025 \\ 0 & 1.5664 & -0.0079 & 0.9871 & 0.0032 \\ 0 & -0.0025 & -0.0262 & 0.0000 & -0.0001 \end{bmatrix}, \\ \Gamma &= \begin{bmatrix} 0.0012 \\ 0.0015 \\ 0.1188 \\ 0.1488 \\ 0.5056 \end{bmatrix}, \quad \Psi = \begin{bmatrix} 0.0456 & 0.0573 \\ 0.0573 & 0.9348 \\ 4.5580 & 5.7114 \\ 5.7114 & 93.2669 \\ -0.1188 & -0.1488 \end{bmatrix}, \\ H &= \begin{bmatrix} 1 & 0 & 0 & 0 & 0 \\ 0 & 1 & 0 & 0 & 0 \end{bmatrix}, \quad \Lambda = [1 \quad 0 \quad 0 \quad 0 \quad 0]. \end{aligned} \tag{33}$$

Table 1. Parameters of the Furuta Pendulum prototype.

Parameter	Description [Unity]	Value
$\hat{J}_1$	Total inertia of the arm axis $[N.m^2]$	1.4064×10^{-3}
$\hat{J}_2$	Total inertia of the rod axis $[N.m^2]$	2.3031×10^{-4}
b_1	Damping coefficient of the arm axis $[N.m.s/rad]$	2.6931×10^{-5}
b_2	Damping coefficient of the rod axis $[N.m.s/rad]$	1.3823×10^{-4}
g	Gravity acceleration $[m/s^2]$	9.81
m_1	Mass of the arm $[kg]$	0.0248
m_2	Mass of the rod $[kg]$	0.0171
L_1	Total length of the arm $[m]$	0.170
L_2	Total length of the rod $[m]$	0.200
l_1	Half of the arm length $[m]$	0.085
l_2	Half of the rod length $[m]$	0.1
L_m	Inductance of the motor's armature $[H]$	4.2380×10^{-4}
R_m	Resistance of the motor's armature $[\Omega]$	1.9658
K_m	Motor constant $[V.s/rad]$	0.05178

The following section discusses the theory used to control the Furuta Pendulum prototype, which is described in Section 2, using the model (32) and (33).

IV. FURUTA PENDULUM STATE FEEDBACK CONTROL

This section describes the strategies used to control the Furuta Pendulum and the theory on which they are based. State feedback control will be used, which considers that all state variables of a system are measurable and available for feedback. In discrete time, the state space model of the system, disregarding the disturb, is given by

$$x(k+1) = \Phi x(k) + \Gamma u(k), \qquad y(k) = Hx(k), \tag{34}$$

where $x(k) \in \mathbb{R}^n$ is the state vector, $u(k) \in \mathbb{R}^m$ is the input vector, and $y(k) \in \mathbb{R}^l$ is the output vector. The matrices $\Phi \in \mathbb{R}^{n\times n}$, $\Gamma \in \mathbb{R}^{n\times m}$, and $H \in \mathbb{R}^{l\times n}$ are constant and known. The pair (Φ, Γ) is considered completely state controllable.

The discrete control law is composed by the linear combination of all state variables. For a system that has only one control input, the control law is given by

$$u(k) = -Kx(k) = -[k_1 \quad k_2 \quad k_3 \ \ldots \ k_n]\begin{bmatrix} x_1(k) \\ x_2(k) \\ x_3(k) \\ \vdots \\ x_n(k) \end{bmatrix}, \tag{35}$$

where $K \in \mathbb{R}^n$ is the gain vector, designed so that the closed-loop system has the desired eigenvalues and presents an adequate response. Considering the system (34) and state feedback (35), the closed loop system has its structure according to Figure 4 and dynamics given by

$$x(k+1) = [\Phi - \Gamma K]x(k). \tag{36}$$

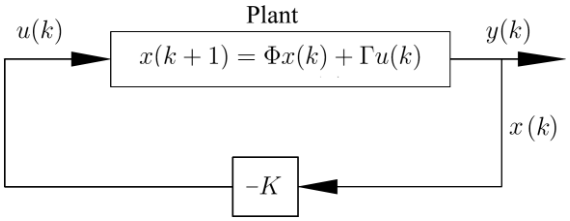

Figure 4. State feedback control [27].

4.1. State Estimator

In practice, it is possible that not all state variables of a real system are measurable and available for feedback. The unavailable state variables, therefore, must be estimated to use the control law (35), what can be done by using a state estimator. This work considers a state predictor estimator, which diagram is shown in Figure 5.

The dynamics of the state estimator is given by

$$\bar{x}(k+1) = \Phi\bar{x}(k) + \Gamma u(k) + L_p[y(k) - H\bar{x}(k)], \tag{37}$$

where L_p is a gain matrix to be determined. This estimator is called predictive because a measure in time k results in state estimation at $k + 1$ [27].

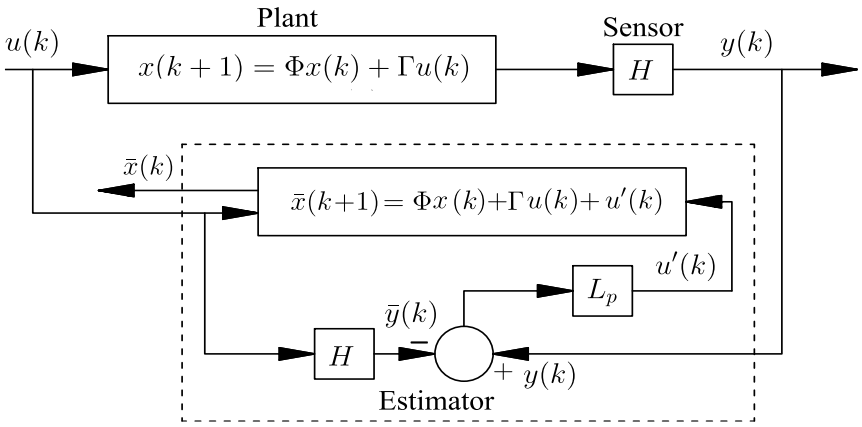

Figure 5. State estimator diagram [27].

Let the error between the estimated state and the real state of the plant be $\tilde{x}(k) = \bar{x}(k) - x(k)$. Then,

$$\tilde{x}(k+1) = \bar{x}(k+1) - x(k+1). \tag{38}$$

Replacing (34) and (37) in (38), it follows that

$$\tilde{x}(k+1) = \Phi\bar{x}(k) + \Gamma u(k) + L_p[y(k) - H\bar{x}(k)] - [\Phi x(k) + \Gamma u(k)].$$

From (34), $y(k) = Hx(k)$, so

$$\tilde{x}(k+1) = \Phi[\bar{x}(k) - x(k)] - L_pH[\bar{x}(k) - x(k)] = [\Phi - L_pH]\tilde{x}(k). \tag{39}$$

If the dynamics (39) is asymptotically stable, the estimation error $\tilde{x} \to 0$ as $k \to \infty$, whatever the value of $\tilde{x}(0)$. For the estimation to be efficient, it is necessary that $\tilde{x}(k)$ converge faster than $x(k)$. For that, the estimator gain L_p must be such that the eigenvalues of $\Phi - L_pH$ are adequate.

Remark 1 *The problem of finding the gain L_p in (39) is similar to finding the gain K in (36). Specifically, consider the system*

$$z(k+1) = \Phi^T z(k) + H^T u(k), \tag{40}$$

with the control law

$$u(k) = -L_p^T z(k). \tag{41}$$

The characteristic equation of the closed-loop system (40) and (41) is $det\left(sI - (\Phi^T - H^T L_p^T)\right) = det\,(sI - (\Phi - L_pH))$, where the latter is the characteristic equation of (39). Thus, the problem of finding the estimator gain L_p in (39) is equivalent to finding the state feedback gain for the system (40) and (41). Therefore, the same methodology used to design the gain K in (36) can be applied to design the gain L_p using the auxiliary system (40) and (41) [33].

4.2. State Feedback Control with State Estimator

Not all state variables are available for feedback in the Furuta Pendulum considered in this paper. Therefore, in order to use the control law (35), the idea is to use the state estimation given by (36). The new feedback control law is given by

$$u(k) = -K\bar{x}(k). \tag{42}$$

A diagram of this control strategy is shown in Figure 6.

The equation describing the system in Figure 6 consists of the dynamics of the estimation error (39) along with the system dynamics (34) and control law (42). Knowing that $\tilde{x}(k) = \bar{x}(k) - x(k)$, one has $\bar{x}(k) = \tilde{x}(k) + x(k)$. Thus, when placed in matrix form, the complete dynamics of the control diagram in Figure 6 become

$$\begin{bmatrix}\tilde{x}(k+1)\\ x(k+1)\end{bmatrix} = \begin{bmatrix}\Phi - L_pH & 0\\ -\Gamma K & \Phi - \Gamma K\end{bmatrix}\begin{bmatrix}\tilde{x}(k)\\ x(k)\end{bmatrix}, \tag{43}$$

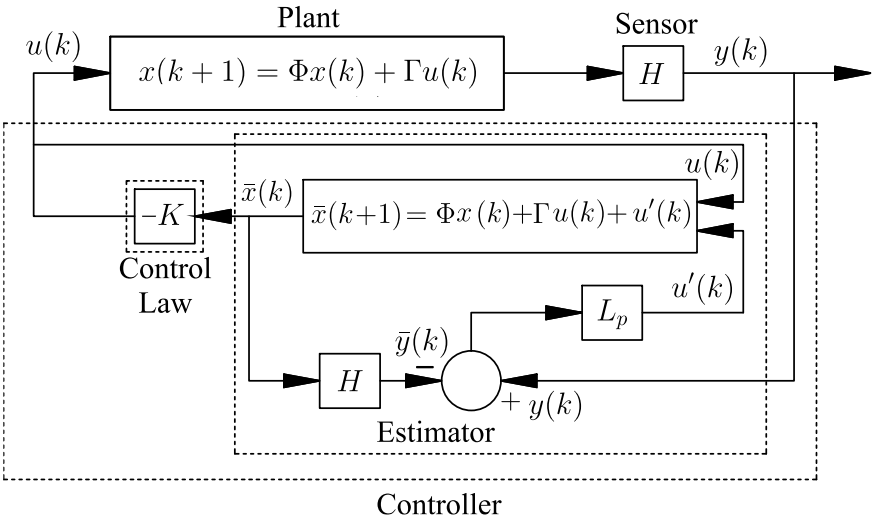

Figure 6. State feedback controller with estimator [27].

which characteristic equation is given by

$$\alpha(z) = det\begin{bmatrix}z\mathrm{I} - \Phi + L_pH & 0\\ \Gamma K & z\mathrm{I} - \Phi + \Gamma K\end{bmatrix} = 0. \tag{44}$$

Since the matrix given in (44) is zero on the upper right-hand side, its characteristic equation can be written as

$$\alpha(z) = det\left[z\mathrm{I} - \Phi + L_pH\right]det[z\mathrm{I} - \Phi + \Gamma K] = \alpha_e(z)\alpha_c(z) = 0, \tag{45}$$

where $\alpha_e(z)$ is the characteristic polynomial of the estimator error (39) and $\alpha_c(z)$ is the characteristic polynomial of the closed-loop system (36). Therefore, the roots of the characteristic polynomial of the complete system consist of a combination of the roots of the characteristic polynomial of the estimator with the roots of the characteristic polynomial of the closed-loop plant, and they do not differ from those obtained assuming that the state of the plant ($x(k)$) is available for state feedback. Consequently, the controller and the estimator can be designed separately and used together. In other words, the system eigenvalues of (45) depend on the eigenvalues of the matrices $\Phi - \Gamma K$ and $\Phi - L_pH$. Thus, the gain matrices K and L_p can be designed independently. In the next sections, the two methods used in this work to obtain these matrices are presented [27].

4.3. Pole Placement

For a discrete-time and completely controllable state system, the closed-loop poles can be placed in any desired position of the Z plane, by means of state feedback, using an appropriate gain matrix [33]. This design method is commonly referred to as Pole Placement.

The closed-loop system given by (36) has characteristic equation

$$det[z\mathrm{I} - \Phi + \Gamma K] = 0. \tag{46}$$

Therefore, the poles of the feedback system depend on K, and can be found using the characteristic equation (46). Thus, it is sufficient to find a matrix K such that the poles of the feedback system coincide with the desired locations [27]. A convenient way to find the gain matrix is to use Ackermann's formula [34] to eliminate the need for calculating the determinant in (46). The Ackermann's formula is given by

$$K = [0, \quad \ldots, \quad 1][\Gamma \quad \Phi\Gamma \quad \Phi^2\Gamma \quad \ldots \quad \Phi^{n-1}\Gamma]\alpha_c(\Phi), \tag{47}$$

where $C = [\Gamma \quad \Phi\Gamma \quad \Phi^2\Gamma \quad \ldots \quad \Phi^{n-1}\Gamma]$ is the controllability matrix, which is nonsingular for a state controllable system; n is the order of the system, and $\alpha_c(\Phi)$ is the desired characteristic equation for the closed-loop system $\alpha_c(z)$ such that z is substituted with the matrix Φ and the independent term is multiplied by the identity matrix of order n.

4.4. Linear Quadratic Regulator (LQR)

The Linear Quadratic Regulator (LQR) method consists of finding a control vector that transfers the system from an initial state to an equilibrium point and for which the quadratic performance index J is minimized. Considering the system presented in (32), the discrete-time performance index J is given by [35]

$$J = \sum_{k=0}^{\infty} x(k)^T Q x(k) + u(k)^T R u(k), \tag{48}$$

where the state weighting matrix, $Q \in \mathbb{R}^{n\times n}$, is positive semidefinite and symmetric, and the control weighting matrix, $R \in \mathbb{R}^{m\times m}$, is positive definite [33]. These matrices represent the relative importance of the state variables in achieving the desired control objectives, such reducing the overshoot in a step response, and the relative importance of the control effort in achieving the desired control objectives, respectively.

Using the control law (35), the performance index (48) is minimized by calculating the gain K by [27]

$$K = (R + \Gamma^T S\Gamma)^{-1}\Gamma^T S\Phi, \tag{49}$$

where S is found by solving the Riccati equation associated with the discrete case

$$S = \Phi[S - S\Gamma(R + \Gamma^T S\Gamma)^{-1}\Gamma^T S]\Phi + Q. \tag{50}$$

4.5. Arm Position Control

Both Pole Placement and LQR control aims to stabilize the system at the equilibrium point $x(k) = 0$. In order to use these control laws and change the angular position of the arm to $\theta_1(t) = \theta_{1r} \neq 0$, a change of variables is proposed. This case is shown in Figure 7.

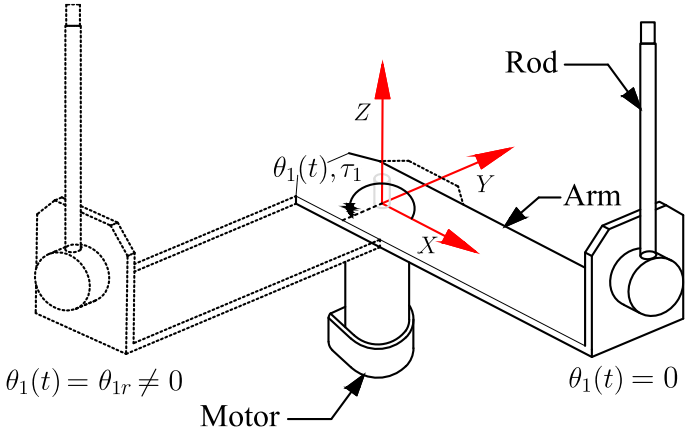

Figure 7. Arm and rod balance positions.

Note that the state $x_r = [\theta_{1r} \quad 0 \quad 0 \quad 0 \quad 0]^T$ is an equilibrium point of the Furuta Pendulum with $u(k) = 0$, i. e., from (33) and (34),

$$x(k+1) = \Phi x_r = x_r. \tag{51}$$

The error between the state of the Furuta Pendulum $x(k)$ and the final equilibrium position x_r is defined as

$$\varepsilon(k) = x(k) - x_r. \tag{52}$$

The idea is to describe the Furuta Pendulum using the new state vector $\varepsilon(k)$. Note that $\varepsilon(k) = 0$ in (52) implies $x(k) = x_r$. Also, when the system is in the equilibrium point one has $x(k) = x(k+1) = x_r$.

From (52), (31) and (51), one has

$$\begin{aligned}\varepsilon(k+1) = x(k+1) - x_r &= \Phi x(k) + \Gamma u(k) - \Phi x_r = \Phi(x(k) - x_r) + \Gamma u(k) \\ &= \Phi\varepsilon(k) + \Gamma u(k).\end{aligned} \tag{53}$$

The control law based in the error $\varepsilon(k)$ in (53) is shown in Figure 8 and given by

$$u(k) = -K\varepsilon(k) = -K[x(k) - x_r]. \tag{54}$$

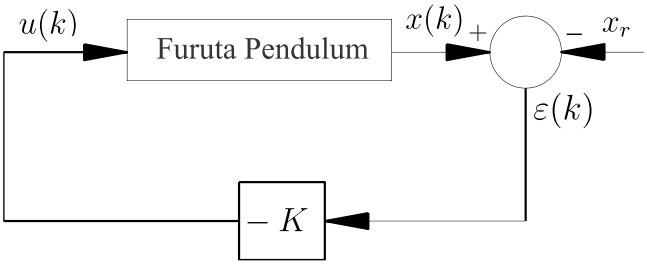

Figure 8. Control diagram used to stabilize the Furuta Pendulum in the equilibrium point $x(k) = x_r$.

By substituting the control law (54) in (53), it follows that

$$\varepsilon(k+1) = \Phi\varepsilon(k) + \Gamma K\varepsilon(k) = [\Phi - \Gamma K]\varepsilon(k). \tag{55}$$

Note that, from (55), the position error has the same dynamics as (36). This indicates that a feedback gain designed to stabilize the dynamics (36) can be effectively used in the control structure depicted in Figure 8 to bring the system state to the desired equilibrium point $x(k) = x_r$. Based on this observation, the control gains are designed in this study by utilizing the dynamics (36), using Pole Placement and LQR, and used in implementing the control structure illustrated in Figure 8.

V. RESULTS

The design of state feedback controllers consists of determining a matrix gain that provides an adequate system response in simulations and experiments. According to Subsection 4.1, as the instrumentation of the Furuta Pendulum system used does not allow the measurement of all the state variables of the model (31), a state predictor estimator was also used to estimate the state variables for feedback. It is important to highlight that the controller and estimator designs follow the same procedures for both adopted control techniques.

In the case of the Pole Placement technique, the design begins with selecting a pole vector in continuous time. Poles on the left half-plane of the complex plane were empirically chosen. Any transient response can reach equilibrium in this condition, characterizing a stable system [33]. Thus, the pole vector in continuous time for the controller is given by

$$p_c = [-6 \quad -7 \quad -8 \quad -9 \quad -10]^T. \tag{56}$$

Regarding the estimator, the empirically selected poles must be farther from the imaginary axis than the controller poles to guarantee state variable estimation [33]. The vector with the chosen poles for the estimator is

$$l_c = [-150 \quad -152 \quad -154 \quad -156 \quad -158]^T. \tag{57}$$

From the vectors given in (56) and (57), the mapping $z = e^{sT_s}$ was used to determine the poles in discrete time, where s is the pole in continuous time, $T_s = 0.02\ s$ is the sampling period, and z is the corresponding pole in discrete time. The following vector, for the controller and estimator, respectively, were obtained

$$p = [0.8869 \quad 0.8694 \quad 0.8521 \quad 0.8353 \quad 0.8187]^T, \tag{58}$$

$$l = [0.0498 \quad 0.0478 \quad 0.0460 \quad 0.0442 \quad 0.0408]^T. \tag{59}$$

The design of the gain matrices K and L_p from (36) and (37), respectively, were calculated using the command 'place' in MatLab®. Considering the poles in (58), and the matrices Φ and Γ in (33), the feedback gain

$$K = [-0.9416 \quad 16.0556 \quad -0.6789 \quad 1.6979 \quad -0.9111] \tag{60}$$

was obtained. Using the poles (59) and the matrices Φ and H from (33), it followed that

$$L_p^T = \begin{bmatrix} 1.8857 & -0.0275 & 44.4812 & -1.2606 & -62.5982 \\ -0.0230 & 1.8822 & -0.7780 & 45.2519 & -88.8423 \end{bmatrix}. \tag{61}$$

Regarding the LQR controller, the quadratic performance index (48) depends on the state weighting matrix, Q, and the control weighting matrix, R. These matrices define the relative importance of the state variables and control inputs in the control design. The matrices were empirically chosen based on the desired performance specifications of the closed loop. For the feedback gain design, these matrices were chosen as

$$Q = \begin{bmatrix} 150 & 0 & 0 & 0 & 0 \\ 0 & 200 & 0 & 0 & 0 \\ 0 & 0 & 5 & 0 & 0 \\ 0 & 0 & 0 & 5 & 0 \\ 0 & 0 & 0 & 0 & 5 \end{bmatrix}, \quad R = [2]. \tag{62}$$

Using the 'dlqr' command in MatLab® and considering the matrices in (33) and (62), the following gain was obtained for the control law (36):

$$K = [-5.0336 \quad 52.1491 \quad -2.9019 \quad 5.5980 \quad 0.0106]. \tag{63}$$

The design of the state estimator was also performed using the LQR technique. In this case, the design matrices were chosen as

$$Q_0 = \begin{bmatrix} 0.0001 & 0 & 0 & 0 & 0 \\ 0 & 0.0001 & 0 & 0 & 0 \\ 0 & 0 & 0.0001 & 0 & 0 \\ 0 & 0 & 0 & 1.000 & 0 \\ 0 & 0 & 0 & 0 & 1.000 \end{bmatrix}, \quad R_0 = 10^{-5} \begin{bmatrix} 0.4540 & 0 \\ 0 & 0.4540 \end{bmatrix}. \tag{64}$$

Considering the matrices in (33) and (63), the following gain was obtained

$$L_p^T = \begin{bmatrix} 1.7997 & -0.0073 & 40.2324 & -0.5225 & -1.0598 \\ -0.0005 & 1.8081 & 0.0157 & 41.4078 & -0.0004 \end{bmatrix}. \tag{65}$$

Remark 2 *Note that this paper considered linear approaches to design the feedback gains and state estimators. Therefore, it is required that the system remains close to its equilibrium point so that the linear approximation remains valid. This fact, a limitation of this approach, must be considered when using the proposed control strategy and was observed during the tests.*

The Pole Placement and LQR controllers were tested in simulations and experiments under two conditions. For simulations, the initial condition was $\Delta\theta_2(t) = -\pi/12\ rad$, with other state variables set to zero, around the unstable equilibrium position $\theta_2(t) = \pi\ rad$. In experiments, the rod was first taken from the stable equilibrium point $\theta_2(t) = 0$ to the inverted position $\theta_2(t) = \pi$ before the controller were activated.

The simulation results, obtained using the scheme in Figure 6 along with ZOH to represent the sampling period of $T_s = 0.02\ s$, are subject to modeling errors and inherent implementation noise when tested in the real prototype.

To quantitatively compare the two controllers, a finite-time version of the ITAE performance index was used, which is given by

$$ITAE = \int_{t_i}^{t_f} te(t)\, dt, \tag{66}$$

where t_i is the initial time, t_f, the final time, $e(t)$, the error between the output of the system, $\theta_1(t)$ and $\theta_2(t)$ and the respective references for each of them. For all experiments and simulations, it was considered $t_i = 10\ s$ and $t_f = 60\ s$. The controller with the best performance will be the one that presents the lowest value of this criterion.

5.1. First Experiment

In the first experiment, the following reference was considered for $\theta_1(t)$:

$$\theta_r(t) = \begin{cases} 0, & 0 \le t < 20, \\ \pi/3, & 20 \le t < 40, \\ 0, & 40 \le t. \end{cases} \tag{67}$$

The simulated results of $\theta_1(t)$, $\theta_2(t)$ and the control signal are presented in Figure 9, while in Figure 10, the results obtained in the real prototype of the Furuta Pendulum are shown, both considering the reference (67). The ITAE values for this experiment are shown in Table 2.

The state feedback with state estimator designed using Pole Placement and LQR were able to stabilize the rod of the Furuta Pendulum in the inverted position ($\theta_2(t) = \pi\ rad$) and track the desired trajectory for the arm angle $\theta_1(t)$, as shown in Figures 9 and 10. It can be seen that the controllers had similar performances in the simulations, but the LQR controller had a slight advantage in the time required for stabilization.

However, in Figure 10, it can be observed that the experimental data showed an oscillatory response around the desired reference, which can be attributed to the nonlinear dynamics, imperfections and noise in the prototype. Specifically, the control designed using Pole Placement exhibited larger oscillation amplitude than the LQR controller.

Based on the information in Figures 9 and 10, the data presented in Table 2 indicated that, in most cases, the LQR controller outperformed the Pole Placement technique in this experiment. The only exception was $\theta_2(t)$ obtained from simulation, where the Pole Placement controller had a slight advantage of less than 10%. Furthermore, it can be observed that the control signal did not saturate since the maximum limit for the motor voltage was $12\ V$.

Table 2. ITAE index (66) considering the reference (67) to $\theta_1(t)$.

Test	Angle	LQR	Pole Placement	LQR.100% / Pole Placement
Simulation	$\theta_1(t)$	24.772	29.029	85.335
	$\Delta\theta_2(t)$	2.445	2.246	108.875
Prototype	$\theta_1(t)$	95.037	161.627	58.800
	$\Delta\theta_2(t)$	13.174	16.201	81.316

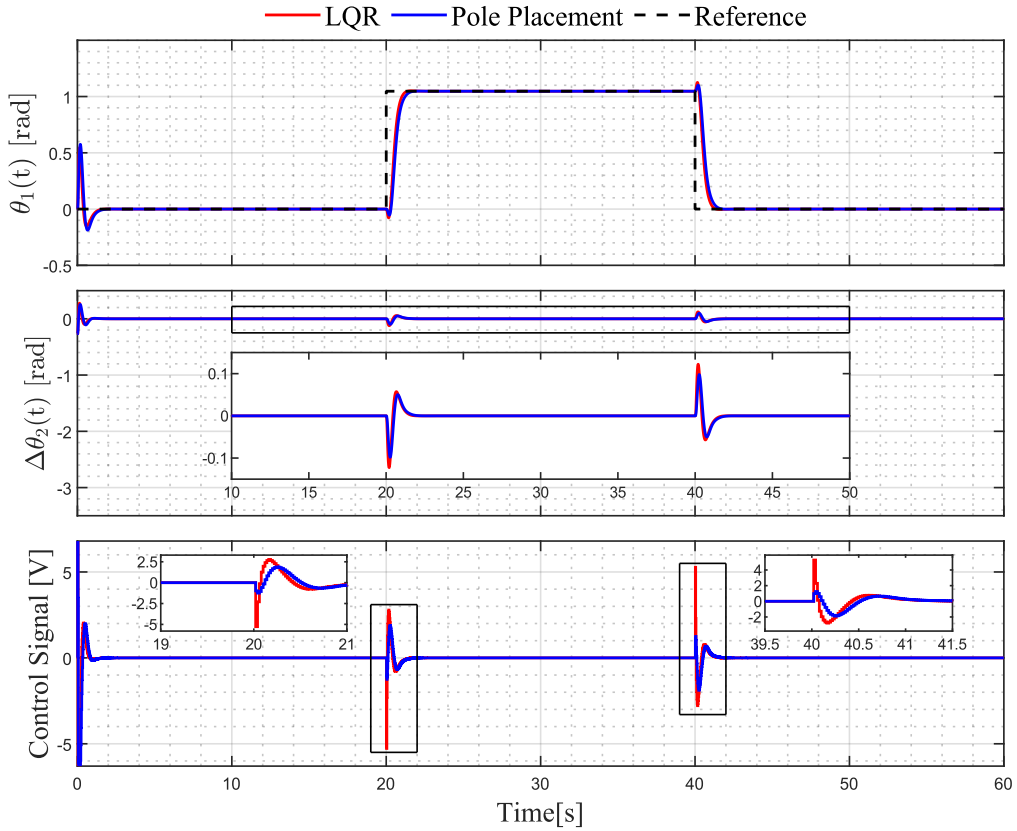

Figure 9. Results obtained by simulation of the Furuta Pendulum considering the reference (67) to $\theta_1(t)$.

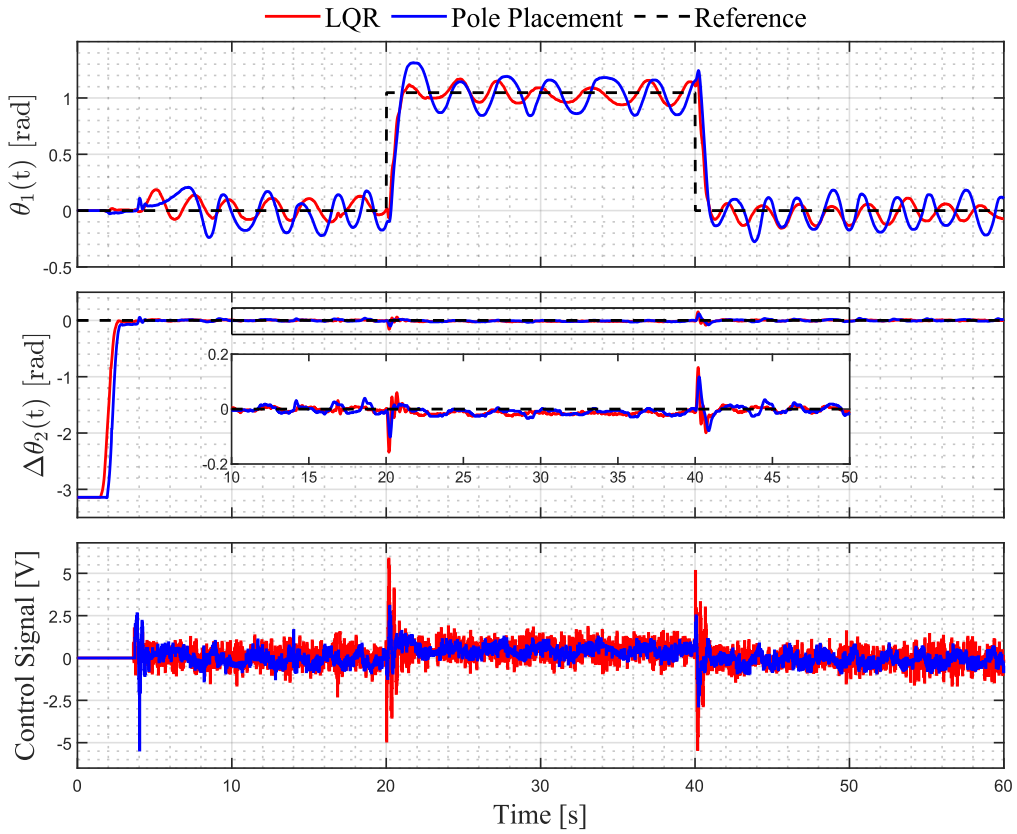

Figure 10. Results obtained experimentally in the Furuta Pendulum considering the reference (67) to $\theta_1(t)$.

5.2. Second Experiment

It can be seen in (27) and (30) that applying an additional signal to the motor voltage generates a current in the motor armature circuit. This current, in turn, influences the dynamics of the angular positions of the rod and arm of the Furuta Pendulum, being added to the term $K_m i(t)$, and acting as a disturbance $\bar{\tau}_1(t)$ in (27).

As this voltage disturbance can be replicated adequately during experiments, it was adopted. In the second experiment, therefore, a disturbance was applied, represented by a signal added to the control action applied to the system, while the reference for the angle of the arm was $\theta_r(t) = 0$. However, a certain time interval was chosen to subject the system to a disturbance, according to

$$d(t) = \begin{cases} 1\,V, & 30 \leq t < 30.5, \\ -1\,V, & 30.5 \leq t < 31, \\ 0, & otherwise. \end{cases} \tag{68}$$

For this experiment, the results of the simulation and the experiment in the real prototype are presented in Figures 11 and 12, respectively.

For both controllers, even with the disturbance (68), the closed-loop system remained stable, with an error that tended to zero. However, it is possible to verify a significant value in the amplitude of oscillation for the controller using Pole Placement in comparison to the LQR one, shown in the simulation (Figure 11). This significant difference, however, was not revealed in the experiment (Figure 12). This behavior is reflected in the values of Table 3, which indicate a superior performance for the controller using LQR in all situations related to the ITAE index.

Table 3. ITAE index (66) considering the disturbance given by (68) in the voltage applied to the motor and reference $\theta_r = 0$.

Test	Angle	LQR	Pole Placement	LQR.100% / Pole Placement
Simulation	$\theta_1(t)$	2.960	14.660	20.190
	$\Delta\theta_2(t)$	0.767	3.974	19.292
Prototype	$\theta_1(t)$	132.914	198.461	66.972
	$\Delta\theta_2(t)$	9.789	16.392	59.722

Finally, it is worth mentioning that, in this experiment, the control signal also did not saturate, for the same reason indicated in the first experiment (Subsection 5.1).

VI. CONCLUSIONS

This study presented the mathematical model obtained through the Lagrangian formulation of a Furuta Pendulum. State feedback control designs using the Pole Placement and LQR techniques were also described in discrete time. Despite the nonlinear dynamics of the Furuta Pendulum, a linearization around the desired equilibrium point was employed in the design procedure. Additionally, a state estimator was used to estimate all unmeasured state variables necessary for feedback in the experimental prototype.

The performance of the controllers was evaluated through two experiments, which confirmed the effectiveness of both control approaches in stabilizing the pendulum around the desired equilibrium. Furthermore, the experimental results validated the mathematical model adopted.

The qualitative analysis of the results indicated that the LQR controller outperformed the Pole Placement controller in most cases. The LQR controller demonstrated smaller oscillations around the reference than the Pole Placement controller in the practical experiments. Additionally, the LQR controller achieved equilibrium slightly faster in simulations.

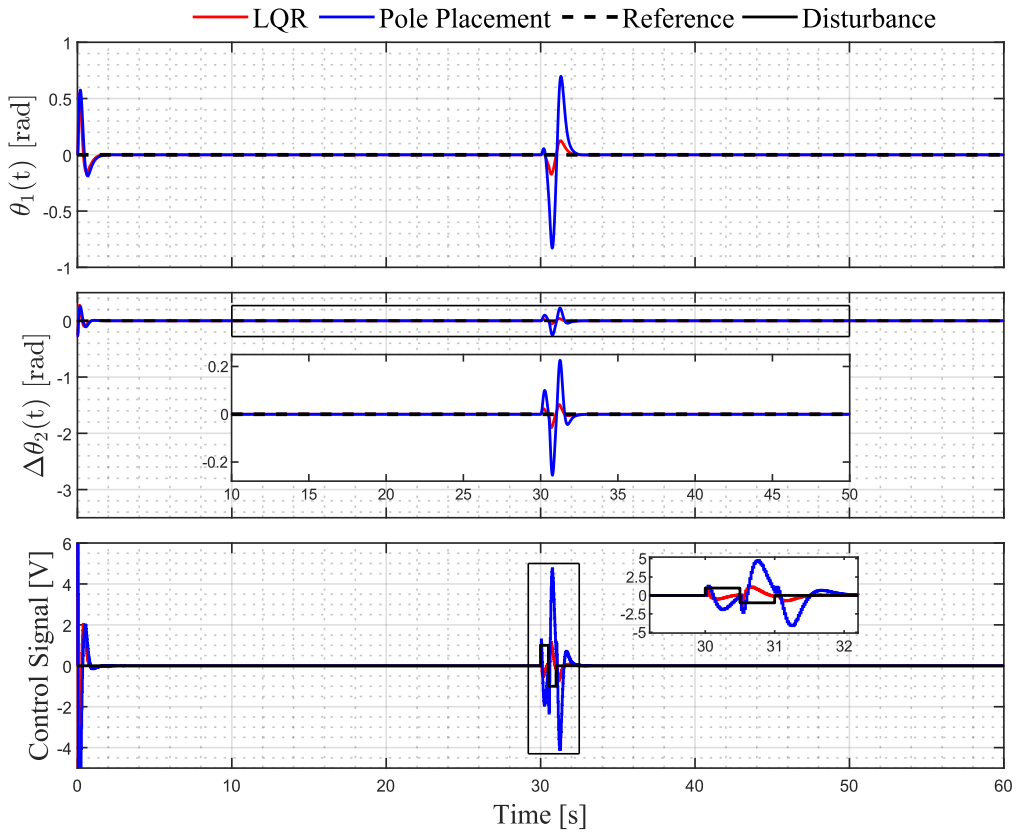

Figure 11. Results obtained by simulation of the Furuta Pendulum considering the disturbance (68) in the control signal.

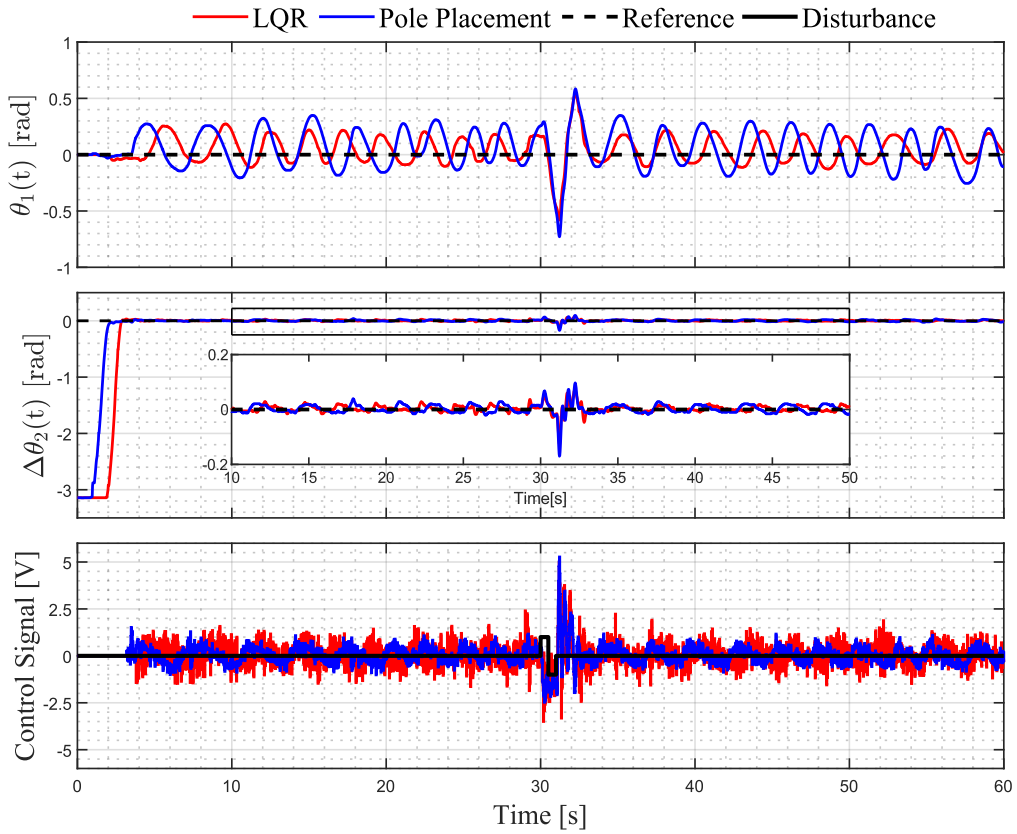

Figure 12. Results obtained experimentally in the Furuta Pendulum considering the disturbance (68) in the control signal.

The ITAE index data referring to the angle $\theta_1(t)$ in the first experiment indicated better performance for the LQR controller compared to the controller using Pole Placement, both in simulation and in the experiment with the prototype. In this case, the biggest difference refers to the real prototype, whose ITAE value for the LQR corresponded at 58.800% of the value for the Pole Placement. Regarding to the angle $\Delta\theta_2(t)$, even in the first experiment, the LQR controller achieved better results in the experiment with the real prototype, but it was surpassed by the controller using Pole Placement in simulation. In this situation, the value obtained by LQR was greater than the value for the Pole Placement in 8.875%.

In relation to the second experiment, the values of ITAE indicated that the LQR controller obtained better performance for both angles, $\theta_1(t)$ and $\Delta\theta_2(t)$, both in simulation and in the experiment with the prototype. In this experiment, the biggest difference between the results was observed for the angle $\Delta\theta_2(t)$ in simulation, whose ITAE value for the LQR corresponded to only 19.29% of the value obtained using the Pole Placement.

In summary, the findings show that the LQR controller provided more satisfactory ITAE index values in seven of eight analyzed scenarios.

A level of robustness for LQR controllers and Pole Placement was also attested, as both were able to maintain the stabilization of the rod in front of the angular variations in the arm of the Pendulum, applied in the experiments. The highest level of robustness was observed in the second experiment, as the rod was maintained in balance in the face of an abrupt action in the system, characterized by a variation in the signal control, applied in a very short time interval (disturbance).

Future studies aim to implement the swing-up control strategy to initialize the experiment with $\Delta\theta_2(t) \neq 0$.

ACKNOWLEDGEMENTS

The authors would like to thank the IFPR Jacarezinho and the UTFPR Cornélio Procópio for their support in the development of this work.

REFERENCES

[1]. Furuta K, Yamakita M, Kobayashi S (1992). Swing-up control of inverted pendulum using pseudo-state feedback. Proceedings of the Institution of Mechanical Engineers, Part I: Journal of Systems and Control Engineering 206(4):263-269.

[2]. Mendez-Flores E, Lopez-Gutierrez JR, Macias-Hidalgo I, Ramirez-Cadena MDJ, Vargas-Martinez A, Lozoya-Santos JDJ, Molina-Gutierrez A (2019). Design, implementation and nonlinear control analysis of a furuta pendulum system. In 2019 4th International Conference on Control and Robotics Engineering (ICCRE) 65-69 IEEE.

[3]. Fu YC, Lin JS (2005). Nonlinear backstepping control design of the furuta pendulum. In Proceedings of 2005 IEEE Conference on Control Applications, 2005. CCA 2005 96-101 IEEE.

[4]. Pivovar LE, Breganon R, Alves UNLT, Ribeiro FSF, Barbara GV, Almeida JPLS, Mendonça M (2020). A tracking system control approach applied on a rotary inverted pendulum model. International Journal of Engineering Research and Applications (IJERA), 10(06):48-56.

[5]. Paredes I, Sarzosa M, Herrera M, Leica P, Camacho O (2017). Optimal-robust controller for furuta pendulum based on linear model. In 2017 IEEE Second Ecuador Technical Chapters Meeting (ETCM) 1:6 IEEE.

[6]. Furka M, Klauco M, Kvasnica M (2019). Stabilization of furuta pendulum using nonlinear mpc. Research Papers Faculty of Materials Science and Technology Slovak University of Technology 27(45):42-48.

[7]. Madrid JLD, Querubín EG, Ospina-Henao PA (2017). Predictive control of a Furuta pendulum. In 2017 IEEE 3rd Colombian Conference on Automatic Control (CCAC). 1-6 IEEE.

[8]. Moreno-Valenzuela J, Aguilar-Avelar C, Puga-Guzmán SA, Santibánez V (2016). Adaptive neural network control for the trajectory tracking of the Furuta pendulum. IEEE transactions on cybernetics 46(12):3439-3452.

[9]. Zabihifar SH, Yushchenko AS, Navvabi H (2020). Robust control based on adaptive neural network for Rotary inverted pendulum with oscillation compensation. Neural Computing and Applications 32:14667-14679.

[10]. Zhang L, Dixon R (2020). Robust nonminimal state feedback control for a Furuta pendulum with parametric modeling errors. IEEE Transactions on Industrial Electronics 68(8):7341-7349.

[11]. Wadi A, Lee JH, Romdhane L (2018). Nonlinear sliding mode control of the Furuta pendulum. In 2018 11th International Symposium on Mechatronics and its Applications (ISMA) 1-5 IEEE.

[12]. Xu J, Niu Y, Lim CC, Shi P (2020). Memory output-feedback integral sliding mode control for furuta pendulum systems. IEEE Transactions on Circuits and Systems I: Regular Papers, 67(6):2042-2052.

[13]. Rigatos G, Siano P, Abbaszadeh M, Ademi S, Melkikh A (2018). Nonlinear H∞ control for underactuated systems: the Furuta pendulum example. International Journal of Dynamics and Control 6:835-847.

[14]. Alves UNLT, Breganon R, Pivovar LE, de Almeida JPLS, Barbara GV, Mendonça M, Palácios RHC (2022). Discrete-Time H∞ Integral Control Via LMIs Applied to a Furuta Pendulum. Journal of Control, Automation and Electrical Systems 33(3):1-12.

[15]. Hamza MF, Yap HJ, Choudhury IA (2017). Cuckoo search algorithm-based design of interval Type-2 Fuzzy PID Controller for Furuta pendulum system. Engineering Applications of Artificial Intelligence 62:134-151.

[16]. Hamza MF, Yap HJ, Choudhury IA, Isa AI, Zimit AY (2016). Simulation studies for stabilization control of Furuta Pendulum System using Cascade Fuzzy PD controller. International Journal of Simulation–Systems, Science and Technology 17(35):1-9.

[17]. Breganon R, Alves UNLT, Ribeiro FSF, Barbara GV, de Almeida JPLS, Pivovar LE, Mendonça M (2021). Development of Inverted Pendulum Systems as Didactical Tools in Courses of Control and Automation Engineering. Holos 5:1-14 (In Portuguese).

[18]. Noh KK, Kim JG, Huh UY (2004). Stability experiment of a biped walking robot with inverted pendulum. In 30th annual conference of IEEE industrial electronics society, 2004. IECON 2004 3:2475-2479 IEEE.

[19]. Mathew NJ, Rao KK, Sivakumaran N (2013). Swing up and stabilization control of a rotary inverted pendulum. IFAC Proceedings Volumes 46(32):654-659.

[20]. Tirmant H, Baloh M, Vermeiren L, Guerra TM, Parent M (2002). B2, an alternative two wheeled vehicle for an automated urban transportation system. In Intelligent Vehicle Symposium, IEEE 2:594-603.

[21]. Ambrose RO, Savely RT, Goza SM, Strawser P, Diftler MA, Spain I, Radford N (2004). Mobile manipulation using NASA's robonaut. In IEEE International Conference on Robotics and Automation, 2004. Proceedings. ICRA 04. IEEE 2:2104-2109.

[22]. Anh ND, Matsuhisa H, Viet LD, Yasuda M (2007). Vibration control of an inverted pendulum type structure by passive mass–spring-pendulum dynamic vibration absorber. Journal of Sound and Vibration, 307(1-2):187-201.

[23]. Alves UNL, Breganon, R, Pivovar LE, de Almeida JPL, Martins LFB, Barbara GV, Mendonça M (2022). Discrete-time modeling and state feedback control of a DC motor with inertial load. Journal of applied research and technology 20(6):718-728.

[24]. Hernández-Guzmán VM, Antonio-Cruz M, Silva-Ortigoza R (2016). Linear state feedback regulation of a furuta pendulum: Design based on differential flatness and root locus. IEEE Access 4:8721-8736.

[25]. Antonio-Cruz M, Hernandez-Guzman VM, Silva-Ortigoza R (2018). Limit cycle elimination in inverted pendulums: Furuta pendulum and pendubot. IEEE Access 6:30317-30332.

[26]. Ortega-Montiel T, Villafuerte-Segura R, Vázquez-Aguilera C, Freidovich L (2017). Proportional retarded controller to stabilize underactuated systems with measurement delays: Furuta pendulum case study. Mathematical Problems in Engineering.

[27]. Franklin GF, Powell JD, Workman ML (1998). Digital control of dynamic systems, Volume 3. Reading, MA: Addison-wesley.

[28]. Craig JJ (2006). Introduction to robotics. Pearson Educacion.

[29]. Hibbeler R C (2004). Engineering mechanics: dynamics. Pearson Educación.

[30]. Halliday D, Resnick R,Walker J (2017). Fundamentals of Physics, Volume 1. John Wiley and Sons.

[31]. Taylor JR (2005). Classical mechanics, Volume 1. Sausalito: University science books.

[32]. Cazzolato BS, Prime Z (2011). On the dynamics of the furuta pendulum. Journal of Control Science and Engineering.

[33]. Ogata K (2010). Modern control engineering, Volume 5. Upper Saddle River, NJ: Prentice hall.

[34]. Ackermann J. (1972). Der entwurf linearer regelungssysteme im zustandsraum. at-Automatisierungstechnik, 20(1-12):297-300.

[35]. Alves UNL, Garcia JPF, Teixeira M, Garcia SC, Rodrigues FB (2014). Sliding mode control for active suspension system with data acquisition delay. Mathematical Problems in Engineering.

Authors

Luiz Eduardo Pivovar received his M.Sc. in Mechanical Engineering from UTFPR (Universidade Tecnológica Federal do Paraná) in 2022. He is a Control and Industrial Processes Professor at IFPR (Instituto Federal do Paraná), Jacarezinho, Paraná, Brazil. His research interests include Dynamic Systems and Mechanical Projects.

Uiliam Nelson Lendzion Tomaz Alves received his Ph.D. in Electrical Engineering from UNESP (Universidade Estadual Paulista) in 2017. He is a Control and Industrial Processes Professor at IFPR (Instituto Federal do Paraná), Jacarezinho, Paraná, Brazil. His research interests include Fuzzy Modeling and Control, LMIs, Robust and Nonlinear Control.

Ricardo Breganon received his Ph.D. in Mechanical Engineering from the University of São Paulo in 2014. He is a Control and Industrial Processes Professor at IFPR (Instituto Federal do Paraná), Jacarezinho, Paraná, Brazil. His research interests include Industrial Automation and Control of Dynamic Systems.

Rodrigo Henrique Cunha Palácios received his Ph.D. in Electrical Engineering from the University of São Paulo in 2016. He is a Professor at the Department of Computing at UTFPR (Universidade Tecnológica Federal do Paraná), Cornélio Procópio, Paraná, Brazil. His research interests include Pattern Recognition, Intelligent Systems, Signal Processing, Fault Identification in Electrical Machines, Robotics and Computer Vision.

Márcio Mendonça received his Ph.D. in Electrical Engineering from the Universidade Tecnológica Federal do Paraná in 2011. He is a Professor at the Department of Electrical Engineering at UTFPR (Universidade Tecnológica Federal do Paraná), Cornélio Procópio, Paraná, Brazil. His research interests include Automation and Industrial Process, acting on the following subjects: Fuzzy Cognitive Maps, Fuzzy Logic, Artificial Neural Networks, Robotic Vision, Intelligent Control, Autonomous Navigation and Swarm Robotics.